BIOCHEMISTRY
including biophysical chemistry & molecular biology

Article

pubs.acs.org/biochemistry

Metal Ion Dependence of the Matrix Metalloproteinase-1 Mechanism

Hao Yang, Katherine Makaroff, Nicholas Paz, Mahesh Aitha, Michael W. Crowder,* and David L. Tierney*

Department of Chemistry and Biochemistry, Miami University, Oxford, Ohio 45056, United States

Supporting Information

ABSTRACT: Matrix metalloproteinase-1 (MMP-1) plays crucial roles in disease-related physiologies and pathological processes in the human body. We report here solution studies of MMP-1, including characterization of a series of mutants designed to bind metal in either the catalytic site or the structural site (but not both). Circular dichroism and fluorescence spectroscopy of the mutants demonstrate the importance of the structural Zn(II) in maintaining both secondary and tertiary structure, while UV−visible, nuclear magnetic resonance, electron paramagnetic resonance, and extended X-ray absorption fine structure show its presence influences the catalytic metal ion's coordination number. The mutants allow us to demonstrate convincingly the preparation of a mixed-metal analogue, Co_CZn_S-MMP-1, with Zn(II) in the structural site and Co(II) in the catalytic site. Stopped-flow fluorescence of the native form, Zn_CZn_S-MMP-1, and the mixed-metal Co_CZn_S-MMP-1 analogue shows that the internal fluorescence of a nearby Trp residue is modulated with catalysis and can be used to monitor reactivity under a number of conditions, opening the door to substrate profiling.

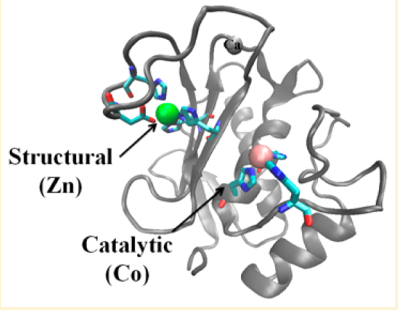

Matrix metalloproteinases (MMPs) are Zn(II)- and Ca(II)-dependent endopeptidases that degrade components of the extracellular matrix, such as collagen, proteoglycans, and fibronectin.[1] They have been broadly categorized into six classes: collagenases, gelatinases, stromelysins, matrilysins, membrane type (MT), and "other" MMPs.[2] The majority of MMPs consist of an N-terminal pro-peptide that maintains the enzyme's latency, a Zn(II)/Ca(II) binding catalytic domain, a variable-length linker, and a hemopexin domain that regulates enzyme activity.[3]

The first reported example of a matrix metalloproteinase (MMP-1)[4] was shown to hydrolyze triple-helical collagens that are essential structural components of connective tissues, such as cartilage, bone, skin, tendons, and ligaments.[5] During catalysis, collagen is initially unwound by the catalytic and hemopexin domains, and a resulting single strand of collagen is fitted into the active site cleft and specifically cleaved to generate three-fourths N-terminal and one-fourth C-terminal fragments.[6−8] Considerable evidence indicates that misregulated MMP-1 is positively correlated with certain cancers,[9−11] and MMP-1 itself can also be used in gene therapy to treat diseases like muscle and hepatic fibrosis and to improve muscle healing.[12−14] This breadth in potential therapeutic scope has sparked considerable effort in the identification of MMP-1 inhibitors.[15−17]

The catalytic zinc (Zn_C) of MMP-1 is coordinated by His218, His222, and His228, along with an uncertain number of solvent molecules, ranging from one to three in inhibitor-free enzyme crystal structures (Figure 1).[18,19] Adjacent to the catalytic Zn(II), but not directly coordinated, Glu219 has been reported to play a critical role in catalysis.[20,21] Also found in the catalytic domain, a second zinc ion (Zn_S), coordinated tetrahedrally by His168, His183, His196, and a monodentate Asp170, helps constrain an S-loop conformation above the catalytic Zn(II) site.[22] Despite their proximity (8−10 Å), the catalytic importance of the structural Zn(II) has not been examined closely.

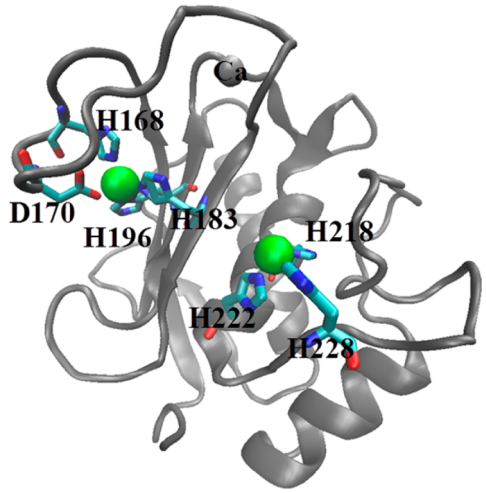

Figure 1. Catalytic domain of MMP-1 (Protein Data Bank entry 1HFC).[55]

The spectroscopic versatility of high-spin Co(II), coupled with functional and structural properties comparable to those of Zn(II),[23] makes Co(II)-substituted MMPs attractive targets for probing the interaction between the catalytic metal center and

Received: April 10, 2015
Revised: May 27, 2015
Published: May 27, 2015

DOI: 10.1021/acs.biochem.5b00379
Biochemistry 2015, 54, 3631−3639

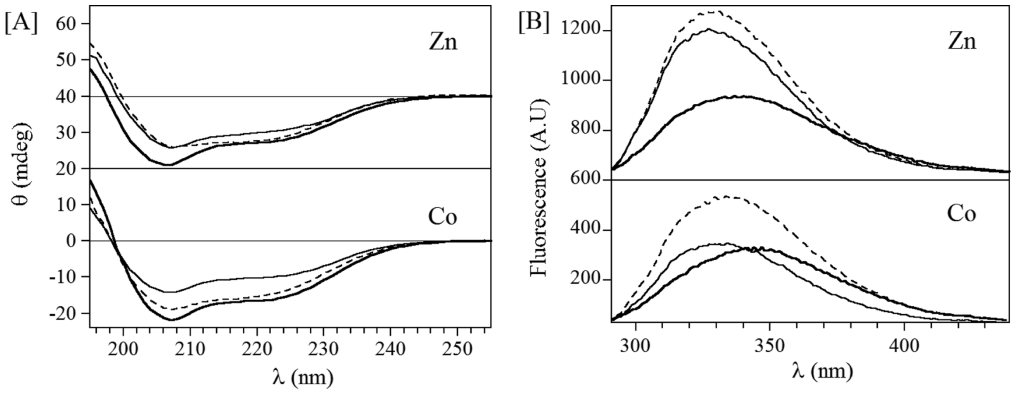

Figure 2. (A) Circular dichroism and (B) fluorescence spectra of Zn(II)- and Co(II)-containing analogues of MMP-1: (thin line) M_CM_S-MMP-1, (thick line) M_C-MMP-1, and (dashed line) M_S-MMP-1.

clinically relevant inhibitors. However, solution characterization of MMPs is sparse. Early work on MMP-3 used optical spectroscopy of the Co(II) enzyme to demonstrate active site binding by the thiol of a potential inhibitor.[24] The Co(II)-substituted analogues of MMP-3 and MMP-7 were examined using only optical spectroscopy and steady state kinetics,[21,24,25] while Co(II)-substituted MMP-12 was used in development of a nuclear magnetic resonance (NMR)-based high-throughput assay.[26] Each of these preceding studies relied on the dicobalt enzyme (Co_CCo_S-MMP-#, based on the notation used here), which requires the deconvolution of overlapping information from an unchanging Co(II)His_3Asp site (Co_S) and a potentially changing Co(II)$His_3(OH_x)_y$ site (Co_C). We report here detailed solution studies of MMP-1, including characterization of a series of mutants designed to bind metal in either the catalytic site or the structural site (but not both). The mutants allow us to demonstrate convincingly the preparation of a mixed-metal MMP-1, with Zn(II) in the structural site and Co(II) in the catalytic site. The detailed characterization of the mixed-metal analogue that is presented will facilitate future studies of binding of ligand and substrate to MMP-1.

MATERIALS AND METHODS

Materials. The plasmid containing the catalytic domain of MMP-1 was a kind gift from K. Brew (Charles E. Schmidt College of Medicine, Florida Atlantic University, Boca Raton, FL). The recombinant enzyme was purified using a previously published procedure.[7] *Escherichia coli* strain BL21(DE3) was purchased from Novagen (Madison, WI). Luria-Bertani (LB) medium was purchased from Invitrogen (Carlsbad, CA). Isopropyl β-D-thiogalactoside (IPTG) was purchased from Anatrace (Maumee, OH). All buffer solutions and growth media were made with Barnstead NANOpure water. Chelex 100 resin (Bio-Rad Laboratories, Hercules, CA) was used to make metal-free buffer, as previously described.[27] Kinetic and spectroscopic studies were conducted in 50 mM HEPES (pH 7.0) containing 100 mM NaCl and 5 mM $CaCl_2$ (hereafter termed simply "buffer"). Fluorogenic peptides FS-6 and DNP-Pro-Leu-Ala-Leu-Trp-Ala-Arg-OH were purchased from Sigma-Aldrich. The reference peptide for FS-6 (Mca-Pro-Leu-OH) was purchased from Enzo Life Science. The QuikChange Site Directed Mutagenesis kit was purchased from Agilent Technology, Inc., and mutations were introduced following the manufacturer's instructions. The primers used to generate the mutations were as follows: M_C-MMP-1 (single mutant H168A), H168A-Forward-CATGATATCTTTTGTCAGGGGAGATGC and H168A-Reverse-GAGAGTTGTCCCGAGCATCTCCCCTG; M_S-MMP-1 (double mutant H218A/H222A), H218A-Forward-CTTACATGGTGTTGCGGCTGCTGAACT, H218A-Reverse-AGAATGGCCGAGTTCAGCAGCCGCAA, H222A-Forward-GGCTGCTGAACTCGGCGCTTCTCTTGGA, and H222A-Reverse-GGAGAGTCCAAGAGAAGCGCCGAGTTCA.

Preparation and Characterization of Co(II)-Substituted MMP-1. Apo-MMP-1 was prepared according to a previously published procedure.[28] Briefly, the purified enzyme was concentrated to 200−300 μM in 4 mL and incubated with ∼4 mL of 4 mM phenanthroline-containing buffer, on ice, for 20 min. Then, 2 mL of 8 M EDTA was added to the solution, and the solution was dialyzed versus 3 × 1 L of buffer (each dialysis step was at least 4 h) containing 50 mM HEPES (pH 7.0), 150 mM NaCl, 2 mM phenanthroline, and 3 mM EDTA, followed by dialysis against buffer alone to remove chelators. The H168A mutant [M_C-MMP-1, where M = Zn(II) or Co(II)] does not bind metal at the structural site, while the H218A/H222A double mutant [M_S-MMP-1, where M = Zn(II) or Co(II)] does not bind metal at the catalytic site; both were prepared by site-directed mutagenesis.[28] The single and double mutants were purified following the same protocol used to purify wild-type (wt) MMP-1. The yield of the double mutant was ∼4 mg/L, similar to that of wt MMP-1, while the yield of the purified H168A single mutant was much lower, ∼1 mg/L. Co(II)-substituted analogues of wt MMP-1 (Co_CCo_S-MMP-1), Co_C-MMP-1, and Co_S-MMP-1 were generated by adding a slight excess of $CoCl_2$ to the metal-free proteins, incubating for 1 h, and dialyzing versus 1 L of metal-free buffer to remove any unbound Co(II).

The mixed-metal hybrid Co_CZn_S-MMP-1 was generated using a method published previously for MMP-3.[25] In brief, 10 mL of Zn_CZn_S-MMP-1 (∼200 μM) was dialyzed against 3 × 1 L of buffer containing 2 mM phenanthroline, 5 mM $CaCl_2$, and 20 mM HEPES (pH 7.5), followed by 2 × 1 L of buffer containing 1 mM $CoCl_2$, 5 mM $CaCl_2$, and 20 mM HEPES (pH 7.5). Lastly, the solution was dialyzed against 5 × 1 L of buffer containing 5 mM $CaCl_2$ and 20 mM HEPES (pH 7.5) to remove unbound phenanthroline and Co(II). A PerkinElmer model 150 inductively coupled plasma atomic emission spectrometer (ICP-AES) was used to measure the metal content of all MMP-1 samples. For the ICP-AES measurements, the protein concentrations were 1 μM, and ICP-AES standards containing Zn(II), Fe(II), and Co(II) at concentrations from 0.5 to 4 μM

DOI: 10.1021/acs.biochem.5b00379
Biochemistry 2015, 54, 3631−3639

were prepared by serial dilution of standard solutions (Fisher Scientific).

Circular Dichroism (CD) and Fluorescence Spectroscopy. CD spectra were recorded on a JASCO J-810 spectropolarimeter, using ~10 μM protein in 50 mM phosphate buffer (pH 7.5). Ten scans were averaged, and the resulting spectra (shown in Figure 2) were analyzed with the online DichroWeb software.[29,30] Fluorescence spectroscopy was performed on a PerkinElmer model LS-55 luminescence spectrometer, with excitation at 280 nm and emission recorded from 290 to 440 nm. Five fluorescence scans of 5 μM protein [buffer consisting of 50 mM HEPES, 5 mM $CaCl_2$, and 100 mM NaCl (pH 7.0)] were averaged to yield the final spectra shown in Figure 2.

Steady State Kinetics. FS-6 was used as the substrate in steady state kinetic studies of the MMP-1 analogues (Scheme 1).

Scheme 1. Chemical Structure of FS-6, with the Scissile Bond Indicated by the Dashed Box

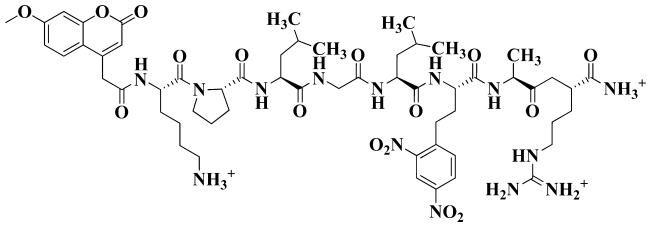

The assays were conducted on a Synergy HT plate reader from Bio-TEK Instruments, Inc.[31] The excitation wavelength was set to 330 nm, and the emission was monitored at 420 nm. The protein concentration was held constant at 10 nM, and substrate concentrations were varied from 10 to 60 μM. The Mca fluorophore of unhydrolyzed FS-6 is quenched by the adjacent DNP group; after cleavage, Mca fluorescence could be recorded by the plate reader. The hydrolyzed substrate concentration at the end of the assay was determined by interpolating from a linear standard curve that correlates Mca-PL-OH fluorescence intensity to a known concentration.

EXAFS Spectroscopy. Samples for EXAFS (approximately 1 mM in protein) were prepared with 20% (v/v) glycerol as a glassing agent. EXAFS samples were loaded in Lucite cuvettes with 6 μm polypropylene windows and frozen rapidly in liquid nitrogen. X-ray absorption spectra were measured at the National Synchrotron Light Source (NSLS), beamline X3B, with a Si(111) double-crystal monochromator. Harmonic rejection was accomplished using a Ni focusing mirror. Fluorescence excitation spectra for all samples were measured with a 31-element solid state Ge detector array. Samples were held at approximately 15 K in a Displex cryostat. EXAFS data collection and reduction were performed according to published procedures.[32] Data were measured in duplicate, six scans at the zinc K-edge and eight scans at the cobalt K-edge, each on two samples from independent purifications. As fits to the two data sets were equivalent, the data were averaged; the experimental spectra presented here are the averaged data sets (12–16 scans per sample). Data were converted from energy to k-space using an E_0 of 9680 eV (Zn) or 7730 eV (Co). Detailed summaries of the fitting results are presented in the Supporting Information.

NMR Spectroscopy. ^{1}H NMR spectra were recorded on 2 mM samples in buffer containing ~10% D_2O. Exchangeable protons were identified by comparison with samples in ~90% D_2O. Spectra were recorded at 290 K on a Bruker ASX200 spectrometer (ν_H = 200.13 MHz), using a frequency switching technique that places a long, low-power (saturating) pulse on the water signal, before moving the transmitter to an arbitrary region of interest.[33] This approach allows accentuation of severely hyperfine-shifted resonances, and often more uniform excitation. Spectra for MMP-1 recorded in this manner were the average of ~200000 transients consisting of 8K points over a 75 kHz spectral window (t_{AQ} = 54 ms, ~16 h per spectrum). The presaturation pulse was typically 100–150 ms (~1 W), centered at the water frequency, while the acquisition pulse was 3 μs at full power, typically centered between 50 and 200 ppm. Prior to Fourier transformation, all free induction decays were apodized using an exponential decay that introduced an additional line width of 30 Hz (0.15 ppm).

EPR Spectroscopy. X-Band EPR spectra were recorded on a Bruker EMX EPR spectrometer equipped with an Oxford Instruments ESR900 helium-flow cryostat. Spectra were recorded at 9.63 GHz ($B_0 \perp B_1$) using an ER4116DM dual-mode cavity, with 10 G (1 mT) magnetic-field modulation at 100 kHz. Spectra were simulated, assuming a fictitious $S' = {}^1/_2$, with *EasySpin*.[34] The simulated g values were then compared with theoretically allowed values for g_{eff} and the rhombicity, assuming an isotropic g-real, using Rhombogram.[35–37]

Stopped-Flow Kinetics. Stopped-flow fluorescence studies using peptide substrate DNP-Pro-Leu-Ala-Leu-Trp-Ala-Arg-OH (DNP = 2,4-dinitrophenyl) and Zn(II)- and Co(II)-containing analogues of the MMP-1 catalytic domain were conducted at 23 °C on an Applied Photophysics spectrophotometer, using an excitation wavelength of 280 nm and a 320 nm high-pass filter on the photomultiplier. A large excess of substrate (20–200 μM) was rapidly mixed with 1 μM enzyme to approximate pseudo-first-order conditions. The data obtained in stopped-flow studies were globally fitted using Dynafit software with the mechanism shown in Scheme 2.[38] All three rate constants were allowed to vary simultaneously, without constraint.

Scheme 2. Reaction Mechanism

$$E + S \underset{k_{-1}}{\overset{k_1}{\rightleftharpoons}} ES \xrightarrow{k_2} E + P$$

RESULTS

Kinetics of the Fully and Singly Loaded Enzymes. The catalytic activities and metal contents of the MMP-1 analogues examined here are listed in Table 1. The catalytic domain of wt MMP-1 (Zn_CZn_S-MMP-1) was purified containing 1.6 equiv of

Table 1. Steady State Kinetic Constants and Metal Contents of MMP-1 Analogues[a]

species	k_{cat} (s^{-1})[b]	K_M (μM)[b]	metal content[c] Zn(II)	metal content[c] Co(II)
Zn_CZn_S-MMP-1	2.1	19	1.6	<0.1
Co_CCo_S-MMP-1	1.9	27	<0.1	1.6
Co_CZn_S-MMP-1	2.3	21	0.8	1.1
Zn_C-MMP-1	0.6	28	0.7	<0.1
Co_C-MMP-1	0.1	18	<0.1	0.7
Zn_S-MMP-1	0		1.1	<0.1
Co_S-MMP-1	0		<0.1	0.9

[a]Substrate, FS-6; see Materials and Methods for conditions. [b]Rate constant, k_{cat} (±0.2), and Michaelis constant, K_M (±8). [c]Metal content in molar equivalents (±0.1).

DOI: 10.1021/acs.biochem.5b00379
Biochemistry 2015, 54, 3631–3639

Zn(II), exhibiting a k_{cat} of 2.1 s^{-1} and a K_m of 19 μM versus FS-6 as a substrate (Scheme 1). The fully Co(II)-substituted enzyme (Co_CCo_S-MMP-1) also bound 1.6 equiv of metal, with steady state kinetic constants similar to those of the Zn(II)-containing enzyme. The mixed-metal analogue, Co_CZn_S-MMP-1, was prepared by dialyzing Zn_CZn_S-MMP-1 against buffer containing phenanthroline, which selectively chelated the more weakly bound catalytic zinc.[21,24,25] Co_CZn_S-MMP-1 prepared in this way bound 0.8 equiv of Zn(II) and 1.1 equiv of Co(II), exhibiting steady state kinetic constants indistinguishable from those of the dizinc and dicobalt enzymes (Table 1). The difference in metal loading between the di-Zn(II) and di-Co(II) enzymes relative to Co_CZn_S-MMP-1 likely reflects the difference in contact time in the final dialysis step. We note that extending this step further reduces the final metal content, suggesting the catalytic site metal ion remains slightly labile.

In an effort to prepare an analogue of MMP-1 capable of binding metal only at the catalytic site (lacking the structural Zn), the H168A single mutant was prepared (Zn_C-MMP-1). It was isolated with 0.7 equiv of Zn(II) bound, exhibiting a K_m similar to that of Zn_CZn_S-MMP-1, but a k_{cat} that was 70% reduced. The Co(II)-substituted version of this mutant (Co_C-MMP-1), prepared by direct addition of Co(II) to the apoenzyme, also bound 0.7 equiv of metal and had a similar affinity for the substrate, but still lower activity. We also note that the yield of this mutant was reduced 4-fold compared to that of wt.

We similarly attempted to prepare a mutant of MMP-1 that binds metal only at the structural site. The H218A mutant still bound 1.7 equiv of Zn(II) and was not pursued further (data not shown). The H218A/H222A double mutant (Zn_S-MMP-1), as predicted, did not exhibit any catalytic activity, though it did bind 1.1 equiv of Zn(II) (Table 1). The Co(II)-substituted version of the double mutant also failed to exhibit catalytic activity, while binding 0.9 equiv of Co(II). From these data, the importance of both metal sites being occupied is readily apparent.

CD and Fluorescence Spectroscopy of MMP-1 Analogues. Because the various analogues of MMP-1 exhibited different steady state kinetic constants, we used CD and fluorescence spectroscopies to probe their secondary structures. As shown in Figure 2A, all of the mutants, and their Co(II)-substituted forms, retain the major secondary structural features of wild-type Zn_CZn_S-MMP-1, although there are minor differences. The CD spectra were analyzed for secondary structural content using the online program DichroWeb.[29,30] On the basis of this analysis, summarized in Table 2, the fold of Zn_CZn_S-MMP-1 is approximately 23% α-helix, 26% β-sheet, and 51% coil, the same as that displayed by Co_CCo_S-MMP-1, within error. The structural analogue, lacking metal at the catalytic site (Zn_S-MMP-1), gave identical results, while the Co(II)-substituted version of this mutant (Co_S-MMP-1) showed an apparent shift in the relative amounts of α-helix and β-sheet (increased by 3% and decreased by 5%, respectively), although this level of change is similar to the experimental error in the technique. The Zn_C-MMP-1 analogue, lacking metal in the structural site, showed exactly the same shift, while the Co(II)-substituted form of this mutant showed the most dramatic change with its α-helical content being 10% higher than that of wt Zn_CZn_S-MMP-1, and a concomitant reduction of the β-sheet content by 9%. While these data may not be quantitative, they clearly show that loss of the structural Zn(II) has some effect on the secondary structure of MMP-1. The data also suggest that the monometallic forms containing Co(II) are slightly altered relative to their Zn(II)-containing counterparts. Most importantly, there is no discernible difference in secondary structure when both metal binding sites are occupied.

Previous studies have shown that the fluorescence properties of tryptophan residues are very sensitive to their local environment, and large changes in emission intensity and fluorescence wavelength are often indicative of changes in tertiary structure.[39,40] The fluorescence emission spectra of the various MMP-1 analogues, using 280 nm excitation, are shown in Figure 2B. Zn_CZn_S-MMP-1 shows a broad peak centered at 327 nm whose intensity increases in the Zn_S-MMP-1 analogue by ~15%. Meanwhile, the intensity of the emission spectrum of the Zn_C-MMP-1 analogue was ~50% of the intensity observed for the dizinc enzyme, and red-shifted to 338 nm. Similar to the Zn(II) enzymes, the Co_S-MMP-1 analogue showed a nearly identical band shape, albeit with greater intensity (35%), compared to that of Co_CCo_S-MMP-1, while Co_C-MMP-1 exhibited a red-shifted emission maximum (345 nm). Unlike those of the zinc enzymes, the emission intensity of the Co_C-MMP-1 analogue was similar to that of Co_CCo_S-MMP-1. The spectra of all three Co(II)-containing enzymes were weaker than those of their Zn(II)-containing counterparts, tailing to longer wavelengths. Both of these observations likely arise because of the optical properties of the incorporated Co(II) ions. Overall, the fluorescence spectra clearly suggest that loss of the structural Zn(II) site alters the tertiary structure of the enzyme, possibly by partially unfolding it near the catalytic site.

EXAFS of MMP-1 Analogues. To examine the effect of the mutations on metal site structure and to ensure the fidelity of Co(II) substitutions, we turned to EXAFS spectroscopy. The best fits to Fourier-transformed k^3-weighted EXAFS data for the various MMP analogues, at the Zn or Co K-edge, are shown in Figure 3 and summarized in Table 3. Detailed fitting results are presented in Figures S1−S6 and Tables S1−S6 of the Supporting Information. The data for wild-type Zn_CZn_S-MMP-1 were best modeled with 4.5 N/O at an average distance of 2.01 Å and 3 His ligands per Zn(II) (Figure S1 and Table S1 of the Supporting Information). Inclusion of 0.5 carbon atom at 2.51 Å, corresponding to Asp170 coordination at the structural site, improved the fit residual by 29%. The EXAFS of Co_CCo_S-MMP-1 was best fit with the same model, including an average of 4.5 N/O donors at 2.03 Å and 3 His ligands per Co(II) (Figure S2 and Table S2 of the Supporting Information). Inclusion of 0.5 carbon scatterer, again corresponding to Asp170, improved the fit residual by 35%. A small increase in first-shell distance is expected, based on the difference in covalent radius, suggesting the two metals adopt the same structure, in both sites.[41]

For comparison, the data for Zn_S-MMP-1 show a relatively high-intensity first-shell peak in its EXAFS Fourier transform

Table 2. Secondary Structure of Zn- and Co-Containing Forms of MMP-1[a]

species	α-helix (%)	β-sheet (%)	random coil (%)
Zn_CZn_S-MMP-1	23	26	51
Zn_C-MMP-1	26	21	53
Zn_S-MMP-1	23	26	51
Co_CCo_S-MMP-1	22	25	53
Co_C-MMP-1	33	17	50
Co_S-MMP-1	26	21	53

[a]The percents of α-helix, β-sheet, and random coil were calculated using CONTIN, available at the Dichroism Web site (see Materials and Methods). Estimated uncertainty of approximately ±1%.

DOI: 10.1021/acs.biochem.5b00379
Biochemistry 2015, 54, 3631−3639

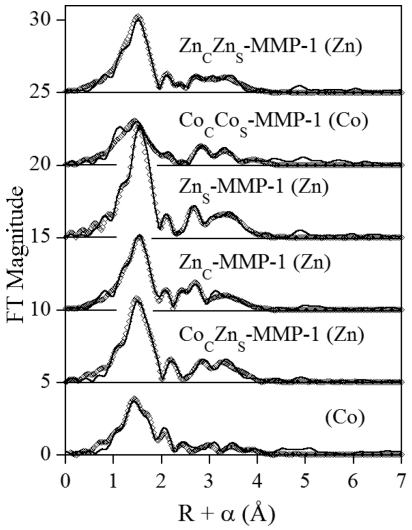

Figure 3. Fourier transforms of MMP-1 EXAFS (—) and their best fits (○). See Table 3 and Figures S1–S6 and Tables S1–S6 of the Supporting Information for details.

Table 3. Best Fits to EXAFS of MMP-1 Analogues[a]

species	model	RM-N/O	fit
ZnCZnS-MMP-1	4.5 N/O (3 His)	2.01	S1-3
CoCCoS-MMP-1	4.5 N/O (3 His)	2.03	S2-3
ZnS-MMP-1	4 N/O (3 His)	1.98	S3-2
ZnC-MMP-1	4.5 N/O (3 His)	2.02	S4-3
CoCZnS-MMP-1 (Zn)	4 N/O (3 His)	2.00	S5-2
CoCZnS-MMP-1 (Co)	5 N/O (3 His), 2 O + 3 N (3 His)	2.08, 1.95 (O), 2.13 (N)	S6-3

[a]See Figures S1–S6 and Tables S1–S6 of the Supporting Information for detailed fitting results.

(Figure 3), reflecting the higher order expected at the structural site. The data were best modeled with 4 N/O per Zn(II) at an average distance of 1.98 Å, including 3 His ligands per Zn(II) (Figure S3 and Table S3 of the Supporting Information). This model is consistent with the structural site defined by crystallography and suggests that the catalytic Zn(II) ion is five-coordinate (based on the reduction in average bond length). Meanwhile, although the preceding data suggested that the overall structure of Zn$_C$-MMP-1 is altered, we measured its EXAFS to see if this translated into an altered metal center (Figure S4 and Table S4 of the Supporting Information). The first-shell data of Zn$_C$-MMP-1 were fitted with 4.5 N/O at an average distance 2.02 Å, including 3 His ligands per Zn(II). This bond length is shorter than would be expected for a homogeneous five-coordinate site and longer than the value of 1.98 Å seen for the structural site mutant. Inclusion of another longer-range scattering interaction significantly improved the fit residual, but the EXAFS could not clearly identify it (see Table S4 of the Supporting Information). On the basis of the crystal structure,[42] a Zn–C interaction would be most likely at 2.49 Å, through coordination of the adjacent Glu219 (this fit is shown in Figure 3). Together with an average bond length that is intermediate to that expected for an increase in coordination number, this suggests there could be a mixture of different Zn(II) centers in Zn$_C$-MMP-1.

EXAFS of the Co$_C$Zn$_S$ analogue provides independent characterization of each metal site, in the same sample. Zinc K-edge EXAFS shows a metal site that is very similar to that of the Zn$_S$-MMP-1 mutant, with 4 N/O donors at 2.00 Å, including 3 His ligands and insignificant improvement in the fit upon inclusion of a second-shell carbon scatterer (Figure S5 and Table S5 of the Supporting Information). Meanwhile, Co K-edge XAS of the same sample shows a substantially longer average first-shell bond length (2.08 Å), consistent with a five-coordinate mixed N/O coordination sphere (Figure S6 and Table S6 of the Supporting Information). Separate shells of 2 O and 3 N lead to a more visually satisfying fit, and a 53% reduction in the fit residual. The separation in the refined distances of 1.96 Å (Co–O) and 2.13 Å (Co–N) is greater than the minimal resolution in the data (ΔR = 0.14 Å), justifying the use of multiple shells. Examination of the Co XANES further supports an average coordination number in the Co$_C$Zn$_S$ analogue higher than that of Co$_C$Co$_S$-MMP-1, based on a substantial reduction in 1s → 3d transition intensity (Figure S7 of the Supporting Information). Together, the Zn and Co K-edge XAS support description of the mixed-metal analogue as a homogeneous Co$_C$Zn$_S$-MMP-1.

Optical Spectroscopy of Co(II)-Substituted MMP-1 Analogues. UV–visible spectra for the four Co(II)-containing analogues (Co$_C$Co$_S$, Co$_C$, Co$_S$, and Co$_C$Zn$_S$) of MMP-1 are shown in Figure 4. The fully Co(II)-substituted enzyme

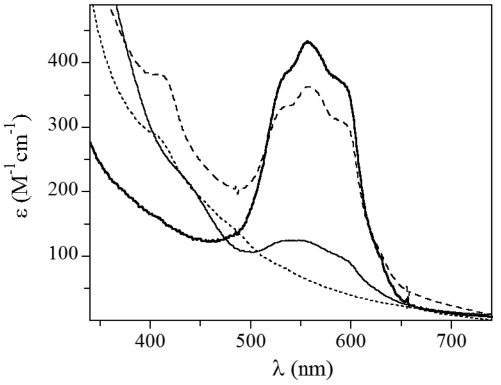

Figure 4. Optical spectra of Co$_C$Co$_S$-MMP-1 (thick solid line), Co$_C$Zn$_S$-MMP-1 (thin solid line), Co$_C$-MMP-1 (dotted line), and Co$_S$-MMP-1 (dashed line).

(Co$_C$Co$_S$-MMP-1, solid line in Figure 4) shows a set of ligand-field transitions with maxima at 533, 555, and 589 nm, whose intensity is suggestive of four coordination (ε = 389, 435, and 373 M^{-1} cm^{-1}, respectively).[43−46] Examination of the Co(II)-substituted mutants suggests that nearly all of the ligand-field intensity can be attributed to Co(II) in the structural site. While Co$_S$-MMP-1 showed a spectrum nearly identical to but slightly weaker than that of the dicobalt wild type, the spectrum of Co$_C$-MMP-1 (dotted line in Figure 4) showed no discernible ligand-field bands. The peak at 415 nm in the Co$_S$-MMP-1 spectrum is most likely due to a small amount of Co(III) (<5%).[47,48]

The optical spectrum of the Co$_C$Zn$_S$ analogue agrees with the mutant spectra shown above, showing only very weak, poorly resolved ligand-field transitions (ε_{max} ~ 120 M^{-1} cm^{-1}). Overall, the optical spectra are consistent with the XAS, suggesting that the structural site metal ion remains four-coordinate in all cases, while Co(II) occupying the catalytic site is five/six-coordinate. The difference between Co$_C$-MMP-1 and Co$_C$Zn$_S$-MMP-1 suggests the catalytic metal may pick up an extra water molecule in the absence of metal in the structural site. These data lend further support to the description of Co$_C$Zn$_S$-MMP-1 as being

DOI: 10.1021/acs.biochem.5b00379
Biochemistry 2015, 54, 3631–3639

uniformly loaded with Co(II) in the catalytic site and Zn(II) in the structural site and suggest the resting catalytic metal ion is five-coordinate.

NMR Spectroscopy of Co(II)-Substituted MMP-1 Analogues. ^{1}H NMR spectroscopy was used to probe the ligand environments in the Co(II)-substituted analogues (Figure 5 and

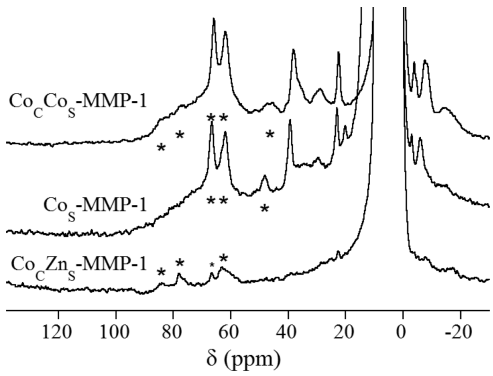

Figure 5. 200 MHz ^{1}H NMR of Co$_C$Co$_S$-, Co$_S$-, and Co$_C$Zn$_S$-MMP-1. Solvent exchangeable protons are marked with asterisks.

Figure S8 of the Supporting Information). Fully substituted Co$_C$Co$_S$-MMP-1 shows a number of signals, both broad and sharp, spanning 100 to −20 ppm. At least five signals (at 83, 78, 66, 62, and 47 ppm, marked with asterisks in Figure 5) are solvent exchangeable and can be readily assigned to the NH protons of Co(II)-bound histidine side chains (the H_2O/D_2O comparisons are presented in Figure S8A of the Supporting Information). The NMR spectrum of Co$_S$-MMP-1 is strikingly similar to that of Co$_C$Co$_S$-MMP-1, lacking the exchangeable intensity at 83 and 78 ppm. On the basis of the crystal structure,[42] the three remaining exchangeable resonances must represent the δ-NH protons on His168 and His183, and the ε-NH proton of His196 at the structural site, although we cannot at present distinguish them. The signals at 36 and 30 ppm can be assigned to either an ε-CH proton of one or more imidazoles or the β-CH_2 proton of His196, either of which is expected to exhibit line widths similar to those of their associated NH protons.[49,50] The two sharper signals at 39 and 23 ppm are tentatively assigned to the geminal β-CH_2 protons of Asp170, which would suggest dissimilar O−C−C−H dihedral angles,[50] again consistent with the crystal structure.[49−51]

In contrast, the ^{1}H NMR spectrum of Co$_C$-MMP-1 was very weak at room temperature (Figure S8A of the Supporting Information), showing a broad set of resonances between 25 and 125 ppm. Four distinct features at 83, 78, 65, and 51 ppm disappeared in D_2O. The 51 ppm resonance is prominent in the Co$_S$-MMP-1 spectrum, and we believe its appearance here indicates a small amount of metal bound at the structural site. An additional sharp resonance, not seen in any of the other analogues, is observed at ∼90 ppm at elevated temperature (Figure S8B of the Supporting Information). Though weak, the Co$_C$-MMP-1 NMR spectrum is consistent with the salient structural features being retained in this analogue and may indicate fluxional structure in the absence of a structural metal ion. The ^{1}H NMR spectrum of Co$_C$Zn$_S$-MMP-1 similarly showed solvent exchangeable signals at 83, 78, 66, and 61 ppm (partially matching those of Co$_C$-MMP-1). These signals shift upfield when the temperature is increased (Figure S8B of the Supporting Information) and are attributed to the NH protons of the three Co(II)-bound histidines from the catalytic site, with a small contaminant from Co(II)-bound histidines at the structural site being responsible for the 66 ppm resonance [supported by EPR (see below)]. Together, the NMR spectra support the assertion that Co$_C$Zn$_S$-MMP-1 is largely homogeneous.

EPR Spectroscopy of Co(II)-Substituted MMP-1 Analogues. The EPR spectrum of wild-type Co$_C$Co$_S$-MMP-1 is complex, appearing to contain at least two signals that can be attributed to MMP-bound high-spin Co(II) (Figure 6). Given

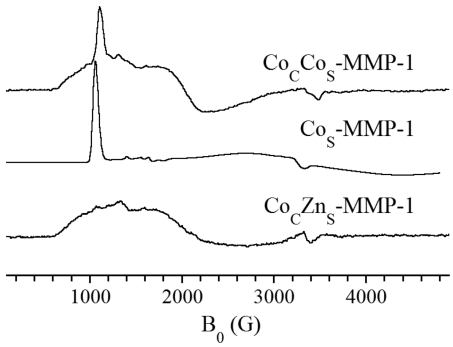

Figure 6. X-Band EPR spectra of Co$_C$Co$_S$-MMP-1 (A, 0.2 mW), Co$_S$-MMP-1 (B, 2 mW), and Co$_C$Zn$_S$-MMP-1 (C, 0.02 mW). The signal near 3400 G is due to a small Cu(II) impurity.

the structural heterogeneity seen in Co$_C$-MMP-1, we did not pursue EPR of this analogue. However, Co$_S$-MMP-1 was shown to be well-behaved, and the sharp low-field feature observed in the Co$_C$Co$_S$-MMP-1 spectrum dominates the spectrum of Co$_S$-MMP-1. In contrast, the low-temperature, low-power EPR spectrum of Co$_C$Zn$_S$-MMP-1 showed a signal that was dominated by the broad component of the Co$_C$Co$_S$-MMP-1 EPR spectrum. A very small contribution from the sharp feature can be seen at elevated power, consistent with the suggestion of some incorporation of Co(II) into the structural site. Although these signals are difficult to quantitate, simple integration suggests <5% of the Co(II) is found in the structural site. The comparison in Figure 6 provides strong support for the description of Co$_C$Zn$_S$-MMP-1 as being largely homogeneous.

Both line shapes have been seen in EPR studies of high-spin Co(II) in proteins,[52−55] and both can easily be reproduced assuming an effective $S' = {}^1/_2$, with observed **g** tensors $[g_{1,2,3}]$ = [6.31, 2.14, 1.54] for Co$_S$-MMP-1 and [6.29, 3.45, 2.30] for Co$_C$Zn$_S$-MMP-1. A simple Rhombogram analysis[37] shows that both sets of g values can be obtained by assuming $S = {}^3/_2$ and $M_S = \pm{}^1/_2$, with an isotropic g_{real} and large E/D (2.28 and 0.31 for Co$_S$-MMP-1 and 2.51 and 0.20 for Co$_C$Zn$_S$-MMP-1, respectively), and indeed, the spectra can be simulated in this way (Figure S9 of the Supporting Information). While neither value of g_{real} is physically meaningful, the ability to match the observed g values using any isotropic g_{real} precludes an appreciably axial **g** tensor. This suggests rhombicity in g_{real}, further precluding determination of a unique set of spin Hamiltonian parameters and any deeper analysis.

Stopped-Flow Fluorescence Kinetic Studies. To probe the reaction mechanism, stopped-flow fluorescence studies were performed on Zn$_C$Zn$_S$-MMP-1 and Co$_C$Zn$_S$-MMP-1 with the substrate DNP-Pro-Leu-Ala-Leu-Trp-Ala-Arg-OH at 23 °C. The kinetic traces contained two phases (Figure 7), a rapid fluorescence decay followed by a slower return phase. The MMP-1 construct employed here bears three Trp residues, Trp109 (14.8 Å from the catalytic metal ion), Trp 141 (10.1 Å), and Trp203 (11.5 Å). We attribute the fluorescence changes to

DOI: 10.1021/acs.biochem.5b00379
Biochemistry 2015, 54, 3631−3639

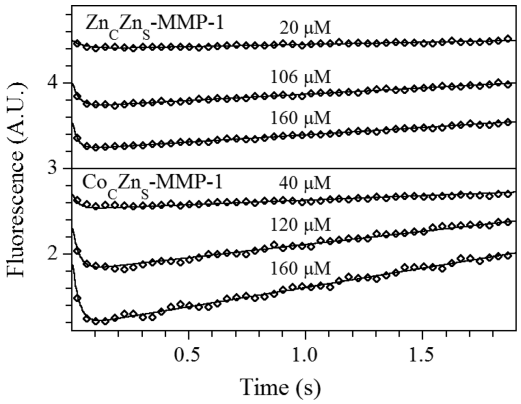

Figure 7. Stopped-flow fluorescence of mixing excess substrate with 1 μM Zn$_C$Zn$_S$-MMP-1 (top) or Co$_C$Zn$_S$-MMP-1 (bottom). Experimental spectra (empty symbols) and fits (filled lines). For the sake of clarity, only 10% of the experimental points are shown.

Trp141, which has been shown to move up to 0.5 Å upon inhibitor binding.[42,56,57] There is no quenching of fluorescence observed when 1 mM enzyme is mixed with 10 mM product (Figure S10 of the Supporting Information), showing the DNP group alone cannot quench the fluorescence of Trp141, suggesting the fluorescence changes we observe are catalytically relevant. The progress curves were fitted using the kinetic mechanism in Scheme 2 (Figure 7), and the microscopic rate constants obtained are summarized in Table 4. The values of k_1 for both Zn$_C$Zn$_S$-MMP-1 and Co$_C$Zn$_S$-MMP-1 are at least 3 orders magnitude lower than the diffusion control limit (>1000 μM^{-1} s^{-1}), suggesting that desolvation or large rearrangement is required before the activated Michaelis complex is formed.[58] The values for k_2, corresponding to the return of fluorescence, would then reflect either product release or bond breaking, and experiments are underway to test this further.

Table 4. Stopped-Flow Kinetics of Zn$_C$Zn$_S$ and Co$_C$Zn$_S$ Analogues of MMP-1

constant[a]	Zn$_C$Zn$_S$	Co$_C$Co$_S$
k_1 (μM^{-1} s^{-1})	0.35	0.17
k_{-1} (s^{-1})	10.7	5.1
k_2 (s^{-1})	2.0	2.5

[a]Constants were globally fitted with Dynafit software using the mechanism in Scheme 1. Uncertainties in k_1, k_2, and k_3 were ±0.01, ±0.2, and ±0.1, respectively.

DISCUSSION

MMPs play an important role in both physiological regulation (skeletal remodeling, wound healing, bone resorption, tissue turnover, and repair) and pathological processes (cancer, arthritis, and cardiovascular disease).[59,60] These validated therapeutic targets have been intensively studied for more than two decades,[61] yet clinical trials of MMP inhibitors have been unsuccessful for a variety of reasons, including missing their drug targets, lack of selectivity, low efficacy, and dramatic side effects.[62,63] While it has been recognized in the past that a Co(II)-substituted MMP could be used to investigate inhibitor binding,[24−26] the presence of two metal sites, only one of which is catalytic, complicates any spectroscopic studies of uniformly substituted enzymes.

To differentiate the spectroscopic characteristics of the catalytic and structural metal ions, His → Ala mutants were prepared and characterized with optical, EXAFS, NMR, and EPR spectroscopies. The Co$_S$-MMP-1 analogue only binds metal at the structural Zn(II) site, supported by the spectroscopic data. The relatively short average bond lengths for both the Zn(II) and Co(II) forms as well as the large extinction coefficient of the ligand-field transitions support a pseudotetrahedral metal site in this analogue, consistent with available crystal structures.[22] In contrast, the analogue lacking metal in the structural Zn(II) site does not appear to be completely viable. CD and fluorescence spectroscopy strongly suggest that M$_C$-MMP-1 has significantly altered secondary and tertiary structure, and it shows 4-fold lower activity. EXAFS of the Zn(II)-containing form, and optical and ^{1}H NMR spectroscopies of the Co(II) form, indicate altered M(II) centers in M$_C$-MMP-1. The residual activity of the M$_C$-MMP-1 mutant suggests conformational flexibility at the catalytic site, consistent with the relatively weaker response of the Co(II) enzyme in solution NMR and UV−vis. The similarity of the Co$_S$-MMP-1 optical and NMR spectra and those of Co$_C$Co$_S$-MMP-1 suggests that some amount of this conformational flexibility is retained in the fully loaded enzyme, consistent with the kinetic observation of a large reorganization following substrate binding. Under these constraints, metal bound at the structural Zn(II) site would serve to shift the catalytic site's conformational equilibrium toward more catalytically competent geometries, rather than simply fixing it into a single conformation.

Regardless of their functional significance, the mutants were critical to deconvolution of the spectra recorded for the Co$_C$Co$_S$ and Co$_C$Zn$_S$ analogues. Selectively introducing Co(II) into the catalytic site, without removing the structural Zn(II) ion, allowed for preparation and characterization of the mixed-metal Co$_C$Zn$_S$-MMP-1. Similar analogues of MMP-3 and MMP-7 were previously reported.[21,25] These analogues were prepared using phenanthroline to chelate Zn(II) from the catalytic site, and it was assumed that the structural Zn(II) site was not accessible to the chelator.[21,24,25] The ratios of Co to Zn in Co$_C$Zn$_S$-MMP-3 and -7 were both reported to be approximately 1:1, but no spectroscopic assessment was conducted. We used a slight modification of this method and were able to obtain a predominant Co$_C$Zn$_S$ analogue of MMP-1. Co$_C$Zn$_S$-MMP-1 exhibited catalytic constants similar to those of the native Zn$_C$Zn$_S$ enzyme. XAS of the mixed-metal enzyme showed a four-coordinate Zn(II) ion, consistent with metal binding at the structural site, and a five-coordinate Co(II) ion bound at the catalytic site. This description is consistent with the weak, broad ligand-field transitions exhibited by Co$_C$Zn$_S$-MMP-1, as well as its ^{1}H NMR and EPR spectra. Most importantly, access to this analogue will allow deeper investigation into substrate and/or inhibitor binding by MMP-1.

Currently, no X-ray structures of an MMP−substrate complex are available, and most of the mechanistic insights into these clinically important enzymes have been gleaned from enzyme−inhibitor X-ray structures. There is a surprising lack of detailed kinetic studies of MMPs, with only one preceding pre-steady state kinetic study, on MT1-MMP.[64] In the study presented here, a conformational change was observed, based on fluctuations in the internal fluorescence of a nearby tryptophan, and this occurred on a catalytically relevant time scale. The small k_1 observed, similar to that seen for MT1-MMP, implies reaction retardation prior to catalysis, such as exclusion of solvent concomitant to substrate binding. These steps might be

DOI: 10.1021/acs.biochem.5b00379
Biochemistry 2015, 54, 3631−3639

particularly energetically expensive when considering the natural substrates of MMPs, which are much larger than the synthetic peptides studied here *in vitro*. Whether the natural substrates, significantly larger in size, will be mechanistically similar to the small synthetic peptides is an aspect of MMP catalysis that we can now examine using pre-steady state kinetics. Experiments to explore the scope of substrate specificity in this manner are underway.

■ ASSOCIATED CONTENT

Supporting Information

Ten figures and six tables showing detailed EXAFS fitting results (Figures S1−S6, Tables S1−S6), Co XANES (Figure S7), H/D-exchanged and temperature-dependent NMR (Figure S8), EPR simulations (Figure S9), and fluorescence intensity versus time for the product of DNP substrate added to enzyme (Figure S10). The Supporting Information is available free of charge on the ACS Publications website at DOI: 10.1021/acs.biochem.5b00379.

■ AUTHOR INFORMATION

Corresponding Authors

*E-mail: tiernedl@miamioh.edu. Phone: (513) 529-8234.
*E-mail: crowdemw@miamioh.edu. Phone: (513) 529-7274.

Funding

This work was supported by the National Institutes of Health (GM093987 to M.W.C. and D.L.T. and P30-EB-009998 to the Center for Synchrotron Biosciences from the National Institute of Biomedical Imaging and Bioengineering, which supports beamline X3B at the National Synchrotron Light Source) and the National Science Foundation (CHE-1151658 to M.W.C. and D.L.T.).

Notes

The authors declare no competing financial interest.

■ ACKNOWLEDGMENTS

Special thanks to Dr. Keith Brew (Charles E. Schmidt College of Medicine, Florida Atlantic University, Boca Raton, FL) for sharing the plasmid containing the catalytic domain of MMP-1 and Dr. Brian Bennett for helpful discussion.

■ ABBREVIATIONS

MMP, matrix metalloproteinase; ZBG, zinc binding group; LB, Luria-Bertani; IPTG, isopropyl β-D-thiogalactopyranoside; HEPES, 2-[4-(2-hydroxyethyl)-1-piperazinyl]ethanesulfonic acid; MCA, (7-methoxycoumarin-4-yl)acetic acid; DNP, 2,4-dinitrophenyl; EXAFS, extended X-ray absorption fine structure.

■ REFERENCES

(1) Nagase, H., and Woessner, J. F. (1999) Matrix metalloproteinases. *J. Biol. Chem. 274*, 21491−21494.
(2) Aureli, L., Gioia, M., Cerbara, I., Monaco, S., Fasciglione, G. F., Marini, S., Ascenzi, P., Topai, A., and Coletta, M. (2008) Structural bases for substrate and inhibitor recognition by matrix metalloproteinases. *Curr. Med. Chem. 15*, 2192−2222.
(3) Tallant, C., Marrero, A., and Gomis-Rüth, F. X. (2010) Matrix metalloproteinases: Fold and function of their catalytic domains. *Biochim. Biophys. Acta 1803*, 20−28.
(4) Gross, J., and Lapiere, C. M. (1962) Collagenolytic activity in amphibian tissues: A tissue culture assay. *Proc. Natl. Acad. Sci. U.S.A. 48*, 1014.
(5) Kadler, K. E., Baldock, C., Bella, J., and Boot-Handford, R. P. (2007) Collagens at a glance. *J. Cell Sci. 120*, 1955−1958.
(6) Manka, S. W., Carafoli, F., Visse, R., Bihan, D., Raynal, N., Farndale, R. W., Murphy, G., Enghild, J. J., Hohenester, E., and Nagase, H. (2012) Structural insights into triple-helical collagen cleavage by matrix metalloproteinase 1. *Proc. Natl. Acad. Sci. U.S.A. 109*, 12461−12466.
(7) Bertini, I., Fragai, M., Luchinat, C., Melikian, M., Toccafondi, M., Lauer, J. L., and Fields, G. B. (2012) Structural basis for matrix metalloproteinase 1-catalyzed collagenolysis. *J. Am. Chem. Soc. 134*, 2100−2110.
(8) Bode, W. (1995) A helping hand for collagenases: The haemopexin-like domain. *Structure 3*, 527−530.
(9) Herrera, I., Cisneros, J., Maldonado, M., Ramírez, R., Ortiz-Quintero, B., Anso, E., Chandel, N. S., Selman, M., and Pardo, A. (2013) Matrix metalloproteinase (MMP)-1 induces lung alveolar epithelial cell migration and proliferation, protects from apoptosis, and represses mitochondrial oxygen consumption. *J. Biol. Chem. 288*, 25964−25975.
(10) Ala-aho, R., and Kähäri, V.-M. (2005) Collagenases in cancer. *Biochimie 87*, 273−286.
(11) Liu, H., Kato, Y., Erzinger, S. A., Kiriakova, G. M., Qian, Y., Palmieri, D., Steeg, P. S., and Price, J. E. (2012) The role of MMP-1 in breast cancer growth and metastasis to the brain in a xenograft model. *BMC Cancer 12*, 583.
(12) Kaar, J. L., Li, Y., Blair, H. C., Asche, G., Koepsel, R. R., Huard, J., and Russell, A. J. (2008) Matrix metalloproteinase-1 treatment of muscle fibrosis. *Acta Biomater. 4*, 1411−1420.
(13) Bedair, H., Liu, T. T., Kaar, J. L., Badlani, S., Russell, A. J., Li, Y., and Huard, J. (2007) Matrix metalloproteinase-1 therapy improves muscle healing. *J. Appl. Physiol. 102*, 2338−2345.
(14) Huard, J., Li, Y., Peng, H., and Fu, F. H. (2003) Gene therapy and tissue engineering for sports medicine. *J. Gene Med. 5*, 93−108.
(15) Puerta, D. T., Griffin, M. O., Lewis, J. A., Romero-Perez, D., Garcia, R., Villarreal, F. J., and Cohen, S. M. (2006) Heterocyclic zinc-binding groups for use in next-generation matrix metalloproteinase inhibitors: Potency, toxicity, and reactivity. *JBIC, J. Biol. Inorg. Chem. 11*, 131−138.
(16) Jacobsen, F. E., Lewis, J. A., and Cohen, S. M. (2006) A new role for old ligands: Discerning chelators for zinc metalloproteinases. *J. Am. Chem. Soc. 128*, 3156−3157.
(17) Jacobsen, F. E., Breece, R. M., Myers, W. K., Tierney, D. L., and Cohen, S. M. (2006) Model complexes of cobalt-substituted matrix metalloproteinases: Tools for inhibitor design. *Inorg. Chem. 45*, 7306−7315.
(18) Iyer, S., Visse, R., Nagase, H., and Acharya, K. R. (2006) Crystal structure of an active form of human MMP-1. *J. Mol. Biol. 362*, 78−88.
(19) Bertini, I., Calderone, V., Fragai, M., Luchinat, C., Maletta, M., and Yeo, K. J. (2006) Snapshots of the reaction mechanism of matrix metalloproteinases. *Angew. Chem., Int. Ed. 45*, 7952−7955.
(20) Johnson, L. L., Pavlovsky, A. G., Johnson, A. R., Janowicz, J. A., Man, C.-F., Ortwine, D. F., Purchase, C. F., White, A. D., and Hupe, D. J. (2000) A rationalization of the acidic pH dependence for stromelysin-1 (matrix metalloproteinase-3) catalysis and inhibition. *J. Biol. Chem. 275*, 11026−11033.
(21) Cha, J., Pedersen, M. V., and Auld, D. S. (1996) Metal and pH dependence of heptapeptide catalysis by human matrilysin. *Biochemistry 35*, 15831−15838.
(22) Maskos, K. (2005) Crystal structures of MMPs in complex with physiological and pharmacological inhibitors. *Biochimie 87*, 249−263.
(23) Maret, W., and Vallee, B. (1993) Cobalt as probe and label of proteins. *Methods Enzymol. 226*, 52.
(24) Salowe, S. P., Marcy, A. I., Cuca, G. C., Smith, C. K., Kopka, I. E., Hagmann, W. K., and Hermes, J. D. (1992) Characterization of zinc-binding sites in human stromelysin-1: Stoichiometry of the catalytic domain and identification of a cysteine ligand in the proenzyme. *Biochemistry 31*, 4535−4540.
(25) Cha, J., Sørensen, M. V., Ye, Q.-Z., and Auld, D. S. (1998) Selective replacement of the catalytic zinc of the human stromelysin-1 catalytic domain. *JBIC, J. Biol. Inorg. Chem. 3*, 353−359.
(26) Bertini, I., Fragai, M., Lee, Y. M., Luchinat, C., and Terni, B. (2004) Paramagnetic metal ions in ligand screening: The CoII matrix metalloproteinase 12. *Angew. Chem., Int. Ed. 43*, 2254−2256.

DOI: 10.1021/acs.biochem.5b00379
Biochemistry 2015, 54, 3631−3639

(27) Hu, Z., Periyannan, G., Bennett, B., and Crowder, M. W. (2008) Role of the Zn1 and Zn2 sites in metallo-β-lactamase L1. *J. Am. Chem. Soc. 130*, 14207−14216.
(28) Wetmore, D. R., and Hardman, K. D. (1996) Roles of the propeptide and metal ions in the folding and stability of the catalytic domain of stromelysin (matrix metalloproteinase 3). *Biochemistry 35*, 6549−6558.
(29) Whitmore, L., and Wallace, B. (2004) DICHROWEB, an online server for protein secondary structure analyses from circular dichroism spectroscopic data. *Nucleic Acids Res. 32*, W668−W673.
(30) Whitmore, L., and Wallace, B. A. (2008) Protein secondary structure analyses from circular dichroism spectroscopy: Methods and reference databases. *Biopolymers 89*, 392−400.
(31) Neumann, U., Kubota, H., Frei, K., Ganu, V., and Leppert, D. (2004) Characterization of Mca-Lys-Pro-Leu-Gly-Leu-Dpa-Ala-Arg-NH_2, a fluorogenic substrate with increased specificity constants for collagenases and tumor necrosis factor converting enzyme. *Anal. Biochem. 328*, 166−173.
(32) Tierney, D. L., and Schenk, G. (2014) X-ray Absorption Spectroscopy of Dinuclear Metallohydrolases. *Biophys. J. 107*, 1263−1272.
(33) Riley, E. A., Petros, A. K., Smith, K. A., Gibney, B. R., and Tierney, D. L. (2006) Frequency-Switching Inversion-Recovery for Severely Hyperfine Shifted NMR: Evidence of Asymmetric Electron Relaxation in High-Spin Co(II). *Inorg. Chem. 45*, 10016−10018.
(34) Stoll, S., and Schweiger, A. (2006) EasySpin, a comprehensive software package for spectral simulation and analysis in EPR. *J. Magn. Reson. 178*, 42−55.
(35) Bennett, B., and Holz, R. C. (1997) EPR studies on the mono- and dicobalt(II)-substituted forms of the aminopeptidase from *Aeromonas proteolytica*. Insight into the catalytic mechanism of dinuclear hydrolases. *J. Am. Chem. Soc. 119*, 1923−1933.
(36) Bennett, B., and Holz, R. C. (1997) Spectroscopically distinct cobalt(II) sites in heterodimetallic forms of the aminopeptidase from *Aeromonas proteolytica*: Characterization of substrate binding. *Biochemistry 36*, 9837−9846.
(37) Hagen, W. R. (2008) *Biomolecular EPR spectroscopy*, CRC Press, Boca Raton, FL.
(38) Kuzmič, P. (1996) Program DYNAFIT for the analysis of enzyme kinetic data: Application to HIV proteinase. *Anal. Biochem. 237*, 260−273.
(39) Vivian, J. T., and Callis, P. R. (2001) Mechanisms of tryptophan fluorescence shifts in proteins. *Biophys. J. 80*, 2093−2109.
(40) Hu, Z., Periyannan, G. R., and Crowder, M. W. (2008) Folding strategy to prepare Co(II)-substituted metallo-β-lactamase L1. *Anal. Biochem. 378*, 177−183.
(41) Huheey, J. E., Keiter, E. A., and Keiter, R. L. (1983) *Inorganic chemistry: Principles of structure and reactivity*, Harper and Row, New York.
(42) Lovejoy, B., Hassell, A. M., Luther, M. A., Weigl, D., and Jordan, S. R. (1994) Crystal structures of recombinant 19-kDa human fibroblast collagenase complexed to itself. *Biochemistry 33*, 8207−8217.
(43) Banci, L., Bencini, A., Benelli, C., Gatteschi, D., and Zanchini, C. (1982) Spectral-structural correlations in high-spin cobalt(II) complexes. In *Structures versus Special Properties*, pp 37−86, Springer, Berlin.
(44) Garmer, D. R., and Krauss, M. (1993) Ab initio quantum chemical study of the cobalt dd spectroscopy of several substituted zinc enzymes. *J. Am. Chem. Soc. 115*, 10247−10257.
(45) Bertini, I., Canti, G., Luchinat, C., and Scozzafava, A. (1978) Characterization of cobalt(II) bovine carbonic anhydrase and of its derivatives. *J. Am. Chem. Soc. 100*, 4873−4877.
(46) Bertini, I., and Luchinat, C. (1983) Cobalt(II) as a probe of the structure and function of carbonic anhydrase. *Acc. Chem. Res. 16*, 272−279.
(47) Breece, R. M., Costello, A., Bennett, B., Sigdel, T. K., Matthews, M. L., Tierney, D. L., and Crowder, M. W. (2005) A five-coordinate metal center in Co(II)-substituted VanX. *J. Biol. Chem. 280*, 11074−11081.
(48) Säbel, C. E., Carbone, R., Dabous, J. R., Lo, S. Y., and Siemann, S. (2011) Preparation and characterization of cobalt-substituted anthrax lethal factor. *Biochem. Biophys. Res. Commun. 416*, 106−110.
(49) Bertini, I., Canti, G., Luchinat, C., and Mani, F. (1981) ^{1}H NMR spectra of the coordination sphere of cobalt-substituted carbonic anhydrase. *J. Am. Chem. Soc. 103*, 7784−7788.
(50) Renault, J. P., Verchère-Béaur, C., Morgenstern-Badarau, I., and Piccioli, M. (1997) Paramagnetic NMR spectroscopy of native and cobalt substituted manganese superoxide dismutase from *Escherichia coli*. *FEBS Lett. 401*, 15−19.
(51) Bertini, I., Turano, P., and Vila, A. J. (1993) Nuclear magnetic resonance of paramagnetic metalloproteins. *Chem. Rev. 93*, 2833−2932.
(52) Makinen, M. W., and Yim, M. B. (1981) Coordination environment of the active-site metal ion of liver alcohol dehydrogenase. *Proc. Natl. Acad. Sci. U.S.A. 78*, 6221−6225.
(53) Carvalho, E., Aasa, R., and Göthe, P.-O. (1996) Electron paramagnetic resonance studies of cobalt-substituted angiotensin I-converting enzyme. *J. Inorg. Biochem. 62*, 147−153.
(54) Cockle, S. A. (1974) Electron-paramagnetic-resonance studies on cobalt(II) carbonic anhydrase-sulphonamide complexes. *Biochem. J. 143*, 703−715.
(55) Martinelli, R. A., Hanson, G. R., Thompson, J. S., Holmquist, B., Pilbrow, J. R., Auld, D. S., and Vallee, B. L. (1989) Characterization of the inhibitor complexes of cobalt carboxypeptidase A by electron paramagnetic resonance spectroscopy. *Biochemistry 28*, 2251−2258.
(56) Grams, F., Crimmin, M., Hinnes, L., Huxley, P., Pieper, M., Tschesche, H., and Bode, W. (1995) Structure determination and analysis of human neutrophil collagenase complexed with a hydroxamate inhibitor. *Biochemistry 34*, 14012−14020.
(57) Spurlino, J. C., Smallwood, A. M., Carlton, D. D., Banks, T. M., Vavra, K. J., Johnson, J. S., Cook, E. R., Falvo, J., Wahl, R. C., and Pulvino, T. A. (1994) 1.56 Å structure of mature truncated human fibroblast collagenase. *Proteins: Struct., Funct., Bioinf. 19*, 98−109.
(58) Fersht, A. (1985) *Enzyme structure and mechanism*, W. H. Freeman and Co., New York.
(59) Vu, T. H., and Werb, Z. (2000) Matrix metalloproteinases: Effectors of development and normal physiology. *Genes Dev. 14*, 2123−2133.
(60) Sternlicht, M. D., and Werb, Z. (2001) How matrix metalloproteinases regulate cell behavior. *Annu. Rev. Cell Dev. Biol. 17*, 463.
(61) Whittaker, M., Floyd, C. D., Brown, P., and Gearing, A. J. (1999) Design and therapeutic application of matrix metalloproteinase inhibitors. *Chem. Rev. 99*, 2735−2776.
(62) Dufour, A., and Overall, C. M. (2013) Missing the target: Matrix metalloproteinase antitargets in inflammation and cancer. *Trends Pharmacol. Sci. 34*, 233−242.
(63) Coussens, L. M., Fingleton, B., and Matrisian, L. M. (2002) Matrix metalloproteinase inhibitors and cancer: Trials and tribulations. *Science 295*, 2387−2392.
(64) Grossman, M., Born, B., Heyden, M., Tworowski, D., Fields, G. B., Sagi, I., and Havenith, M. (2011) Correlated structural kinetics and retarded solvent dynamics at the metalloprotease active site. *Nat. Struct. Mol. Biol. 18*, 1102−1108.

DOI: 10.1021/acs.biochem.5b00379
Biochemistry 2015, 54, 3631−3639